Calendar and cycle aging dataset for lithium-ion batteries with multi-SOC electrochemical impedance spectroscopy measurements

Muhammad Aadil Khan , Colin Chu , Simona Onori

PII: S2352-3409(25)01003-0
DOI: https://doi.org/10.1016/j.dib.2025.112282
Reference: DIB 112282

To appear in: *Data in Brief*

Received date: 8 September 2025
Revised date: 14 October 2025
Accepted date: 10 November 2025

Please cite this article as: Muhammad Aadil Khan , Colin Chu , Simona Onori , Calendar and cycle aging dataset for lithium-ion batteries with multi-SOC electrochemical impedance spectroscopy measurements, *Data in Brief* (2025), doi: https://doi.org/10.1016/j.dib.2025.112282

Data in Brief
Open access
Article template

ARTICLE INFORMATION

Article title

Calendar and cycle aging dataset for lithium-ion batteries with multi-SOC electrochemical impedance spectroscopy measurements

Authors

Muhammad Aadil Khan[a], Colin Chu[b], Simona Onori[a,*]

Affiliations

[a] Department of Energy Science and Engineering, 367 Panama St, Stanford University, Stanford, CA 94305

[b] The Nueva School, 131 E 28th Avenue, San Mateo, CA 94403

Corresponding author's email address and Twitter handle

sonori@stanford.edu

Keywords

Lithium-ion batteries, calendar aging, cycle aging, battery health, reference performance tests, electrochemical impedance spectroscopy

Abstract

This paper presents a comprehensive dataset of 22 NMC/graphite lithium-ion batteries subjected to both calendar and cycle aging under controlled operating conditions. The cells were aged at 0 °C, 25 °C, and 40 °C for a duration of 90 days. Periodic reference performance tests (RPTs) were conducted throughout the aging process. Each RPT included a capacity test and an electrochemical impedance spectroscopy (EIS), both performed at 25 °C. EIS was repeated at state-of-charge (SOC) values of 0%, 25%, 50%, 75% and 100%. Cycle-aged cells were operated between various voltage limits at two distinct charging rates, while calendar-aged cells were stored at either 80% or 100% state-of-charge (SOC). This dataset captures a diverse range of degradation pathways. It can be used to develop and validate battery aging models, state-of-health (SOH) estimation algorithms, and support the design of predictive maintenance strategies for lithium-ion battery systems.

Data in Brief
Open access
Article template

SPECIFICATIONS TABLE

Subject	Electrical and Electronic Engineering
Specific subject area	Calendar and cycle aging dataset for lithium-ion batteries with multi-SOC electrochemical impedance spectroscopy measurements
Type of data	Table.
Data source location	Institution: Stanford Energy Control Lab, Energy Science and Engineering Department, Doerr School of Sustainability, Stanford University. City, State: Stanford, California. Country: United States of America. Latitude and longitude for collected samples/data: (37.426666918636386, -122.17397631867011).
Data accessibility	Repository name: Open Science Framework Data identification number: DOI 10.17605/OSF.IO/J2SN4 Direct URL to data: https://osf.io/j2sn4/
Related research article	Khan, M. A., Thatipamula, S., & Onori, S. (2024). Onboard Health Estimation using Distribution of Relaxation Times for Lithium-ion Batteries. *IFAC-PapersOnLine*, *58*(28), 917-922.[1]

VALUE OF THE DATA

- This dataset provides characterization data for 22 cells that were either calendar-aged or cycle-aged at various operating conditions including temperature, charge rate, and state-of-charge (SOC) range (voltage limits).
- The cycle-aged cells were subjected to one of 18 different combinations of operating conditions, while the calendar-aged cells experienced one of 6 different combinations. This design yields a diverse dataset encompassing a wide range of degradation pathways.

Data in Brief
Open access
Article template

- Reference performance tests (RPTs) consist of a capacity test at 0.2C in charge and 1C in discharge and electrochemical impedance spectroscopy (EIS) at 0%, 25%, 50%, 75%, and 100% SOC. Both RPTs are performed at 25 °C.
- The inclusion of EIS measurements for both calendar-aged and cycle-aged cells makes this dataset particularly valuable for the design of advanced state-of-health (SOH) monitoring algorithms. To the best of the authors' knowledge, it is unique in combining diverse aging modes and operating conditions with comprehensive characterization data.

BACKGROUND

As the adoption of electric vehicles (EVs) continues to grow, reliable and effective diagnostic tools remain essential for monitoring cell degradation and understanding aging mechanisms [2]. Since lithium-ion batteries undergo complex electrochemical reactions, data from various aging conditions is key for the effective deployment of robust battery management systems. Table 1 provides a list of publicly available EIS datasets that include both calendar and cycle aging, as well as those featuring cycle aging only. In calendar and cycle-aging datasets, the EIS is performed only at a single temperature, with SOC fixed at 50% or conducted at a few discrete SOC points. As a result, these datasets exhibit low granularity in the operating conditions for EIS. In contrast, datasets without calendar aging feature EIS measurements at one or multiple temperatures and SOC points. While cycling-only datasets offer higher granularity in the operating conditions for EIS, they do not capture the effects of calendar aging. The present dataset bridges this gap by combining both calendar and cycle-aging with high granularity in the operating conditions for EIS measurements. This research presents capacity and EIS data from nickel-manganese-cobalt (NMC)/graphite cells, providing valuable insights into battery aging across a wide range of frequencies, SOC ranges, temperatures, and aging durations. Furthermore, the dataset can be used in various applications, including the training and evaluation of diagnostic and prognostic models for battery health estimation [3].

Table 1: Calendar & cycling, and cycling-only EIS datasets.

Dataset	Cells	Chemistry	Aging type	EIS temperature	EIS SOC
Saha et al.[4]	34	NCA	Cycling	24, 43	60
Kollmeyer et al.[5]	1	NCA	Cycling	0, 10, 20, 25, 40	Every 5% SOC
Bessman et al.[6]	12	NMC111	Calendar & Cycling	25	50
Raj et al.[7]	28	NCA	Calendar & Cycling	25	20, 50, 80
Gasper et al.[8]	32	NMC	Calendar & Cycling	25	50
Goldammer et al.[9]	39	NMC	Calendar & Cycling	25	20.40. 60, 80
Mohtat et al.[10]	21	NMC	Cycling	25	Every 10% SOC
Pozzato et al.[11]	10	NMC	Cycling	25	20, 50, 80
Rashid et al.[12]	25	NMC811	Cycling	15, 25, 35	5, 20, 50, 70, 95

Data in Brief
Open access
Article template

DATA DESCRIPTION

The dataset consists of 22 prismatic NMC/graphite cells with a nominal capacity of 5 Ah that were either calendar-aged or cycle-aged at various operating conditions. The aging campaign spanned 90 days, during which five different RPTs consisting of capacity tests and EIS at 25 °C were conducted. Table 2 lists the technical specifications of the cells.

Table 2: Technical specifications of NMC/graphite cell.

Manufacturer	Nuvoton
Measurement By	KRI, Inc.
Positive electrode	NMC
Negative electrode	Graphite
Form Factor	Prismatic
Nominal capacity (Q_{nom})	5 Ah
Charge cutoff voltage ($V_{chg,cutoff}$)	4.2 V
Discharge cutoff voltage ($V_{dch,cutoff}$)	2.5 V

The aging campaign is illustrated in Figure 1. Prior to the campaign, an initial assessment (RPT 0) was performed. It included a capacity test and multiple EIS at five SOC values. Afterwards, the cells were either calendar or cycle-aged at 0 °C, 25 °C, and 40 °C. The temperature set points were selected to reflect realistic battery usage conditions while ensuring experimental safety. Since the thermal chambers were a shared resource, data collection at additional temperature set points was not feasible. On day 10, a second RPT was performed to characterize degradation. This was followed by 10 additional days of aging, after which RPT 2 was performed on day 20. RPT 3 was conducted after 20 days of aging, and RPT 4 after 50 days of aging. Table 3 summarizes the specifications of the RPTs. The capacity tests were performed by charging the cells at 0.2C using a constant current-constant voltage (CCCV) protocol, denoted as 0.2C:CCCV, from 0% to 100% SOC and discharging at 1C using a constant-current (CC) protocol, denoted as 1C:CC, from 100% to 0% SOC. For EIS, the test is performed using a range of frequencies between 0.1 Hz and 20 kHz using four points per decade. Each EIS test was repeated at 0%, 25%, 50%, 75%, and 100% SOC for all the cells. These five SOC points were chosen to span the full SOC range in 25% increments while keeping the experimental campaign within budget constraints. Hence, increasing the granularity of the SOC points for EIS was not considered practical.

Data in Brief
Open access
Article template

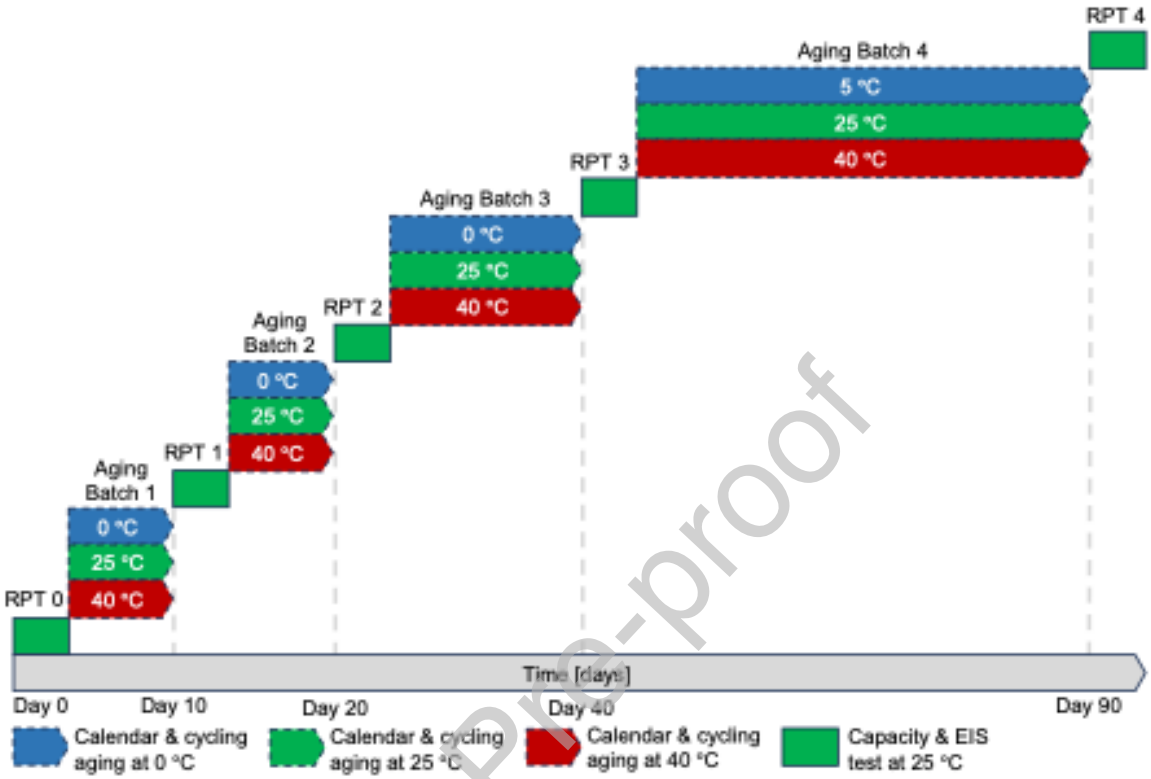

Figure 1: Overview of the 90-day aging campaign. The campaign began with an initial assessment of the cells, consisting of a capacity test and EIS (denoted as RPT 0 on day 0), followed by Aging Batch 1 conducted at 0 °C, 25 °C, and 40 °C. Subsequently, RPT 1 and RPT 2 were performed after Aging Batch 1 and Aging Batch 2, respectively. This sequence of tests was repeated four times in total, concluding the campaign on day 90. All RPTs were conducted at 25 °C, and each aging batch included both calendar-aged and cycle-aged cells.

Table 4 summarizes the operating conditions during aging for all cells, namely temperature values, charging C-rates, and voltage limits. Calendar-aged cells were stored at either 80% or 100% SOC across all three temperatures (0 °C, 25 °C, and 40 °C). Temperature control was implemented at the thermal chamber level. Cycle-aged cells were charged using either 0.2C:CCCV or 1C:CC protocol within one of the following voltage ranges: 2.5–4.2 V, 2.5–4.1 V, 2.5–4.15 V, or 3.0–4.15 V (the corresponding SOC ranges also provided in Table 3). Cells S2 and S18 were excluded from the dataset due to data collection errors during the experimental campaign, resulting in missing data. Cell S2 only included measurements up to Day 20 and Cell S18 only up to Day 40.

Data in Brief
Open access
Article template

Table 3: RPT specifications. The capacity tests in charge and discharge were conducted within the voltage range of 4.2 to 2.5 V (100% to 0% SOC) while EIS tests were conducted at five SOC points. Both tests were carried out at 25 °C.

RPT Type	Test settings	SOC	Temperature
Capacity test	0.2C:CCCV charge 1C:CC discharge	0% to 100% 100% to 0%	25 °C
EIS	0.1 Hz to 20 kHz	0%, 25%, 50%, 75%, 100%	25 °C

Table 4: Aging campaign specifications for all cells in the dataset. While cycle-aged cells shared the same discharge rate, the remaining operating conditions differed among cells for both aging types.

Cell	Aging Type	SOC Range	Voltage Limits	Charge Rate	Discharge Rate	Temperature
S1	Calendar-Aged	100% Fixed	4.2V	–	–	40 °C
S3		100% Fixed	4.2V	–	–	0 °C
S4		80% Fixed	4.1V	–	–	40 °C
S8		80% Fixed	4.1V	–	–	25 °C
S9		80% Fixed	4.1V	–	–	0 °C
S6	Cycle-Aged	0-100%	2.5-4.2V	0.2C:CCCV	1C:CC	25 °C
S15		0-80%	2.5-4.1V	0.2C:CCCV		
S16		10-90%	3.0-4.15V	0.2C:CCCV		
S17		0-100%	2.5-4.2V	1C:CC		
S19		10-90%	2.5-4.15V	1C:CC		
S7	Cycle-Aged	0-100%	2.5-4.2V	0.2C:CCCV	1C:CC	40 °C
S20		10-90%	2.5-4.1V	0.2C:CCCV		
S21		0-80%	3.0-4.15V	0.2C:CCCV		
S22		0-100%	2.5-4.2V	1C:CC		
S23		0-80%	2.5-4.1V	1C:CC		
S24		10-90%	3.0-4.15V	1C:CC		
S5	Cycle-Aged	0-100%	2.5-4.2V	0.2C:CCCV	1C:CC	0 °C
S10		0-80%	2.5-4.1V	0.2C:CCCV		
S11		10-90%	3.0-4.15V	0.2C:CCCV		
S12		0-100%	2.5-4.2V	1C:CC		
S13		0-80%	2.5-4.1V	1C:CC		
S14		10-90%	3.0-4.15V	1C:CC		

The initial charge and discharge capacities of all the cells were obtained from the capacity test conducted during RPT 0 and are presented in Fig. 2. The initial charge capacities were relatively uniform across the dataset, while the discharge capacities exhibited greater variation among cells, indicating differences in available capacity under discharge conditions. Deviation from the mean was minimal for the charge capacities. Notably, the mean initial discharge capacity was approximately 0.09 Ah higher than the mean

Data in Brief
Open access
Article template

initial charge capacity, which may be attributed to initial formation effects or minor measurement asymmetries between the charge and discharge processes. This baseline characterization provides a reference point for the subsequent aging analysis.

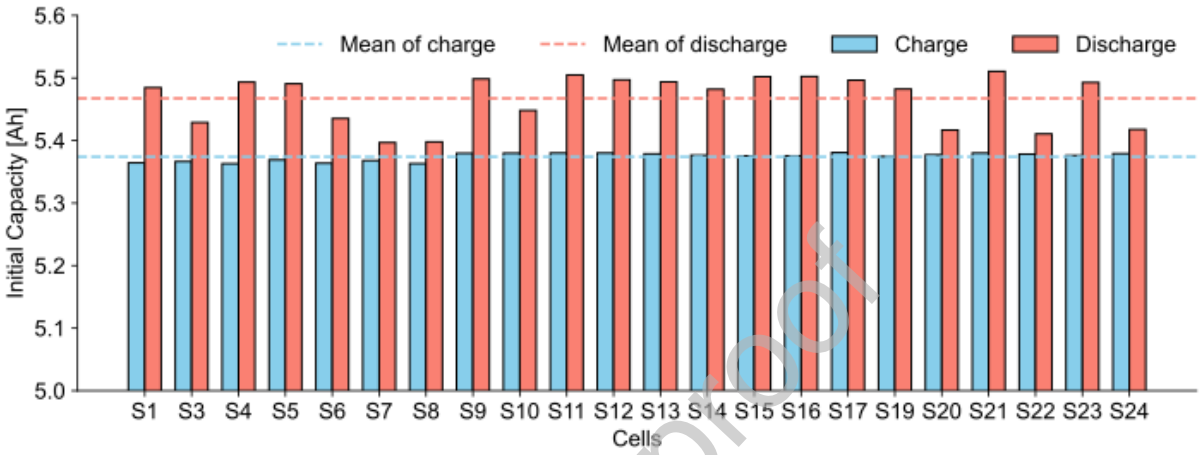

Figure 2: Bar plot of the initial charge and discharge capacity for all cells. The initial charge capacities were consistent across cells and close to the mean initial charge capacity, whereas the discharge capacities showed greater variation. The mean initial discharge capacity was approximately 0.09 Ah higher than the mean initial charge capacity.

The charge and discharge capacity curves resulting from aging are shown in Fig. 3a and 3c, respectively, for all the cells. The cells exhibited a wider spread with aging, with Cell S22 undergoing the greatest degradation in the dataset. The histogram in the inset of Fig. 3a shows the distribution of initial charge capacity, which shows a bimodal distribution around the mean. Similarly, for discharge, the initial capacity distribution was bimodal with more cells present at a higher capacity than the mean. Fig. 3b and 3d show the charge and discharge capacity curves plotted against the equivalent full cycles (EFC) for all cycle-aged cells. EFC was calculated as

$$\text{EFC} = \frac{\text{Ah per day} \times \text{Aging days}}{2 \cdot \text{Q}_{\text{nom}}}.$$

This normalization facilitates a comparison across cells subjected to different cycling intensities. While some cells accumulated a higher number of cycles than others, the extent of degradation is not solely determined by cycle count. Cells, such as cell S7, that operated under harsher conditions—for example, 40 °C or cycled between 4.2 to 2.5 V (complete voltage range)—exhibited greater capacity loss even with fewer accumulated cycles. The distribution of initial charge capacity in Fig. 3b was left-skewed, with more cells present at or above the mean capacity. Similarly, the initial discharge capacity distribution in Fig. 3d remained bimodal after excluding calendar-aged cells, with more cells above the mean discharge capacity.

Data in Brief
Open access
Article template

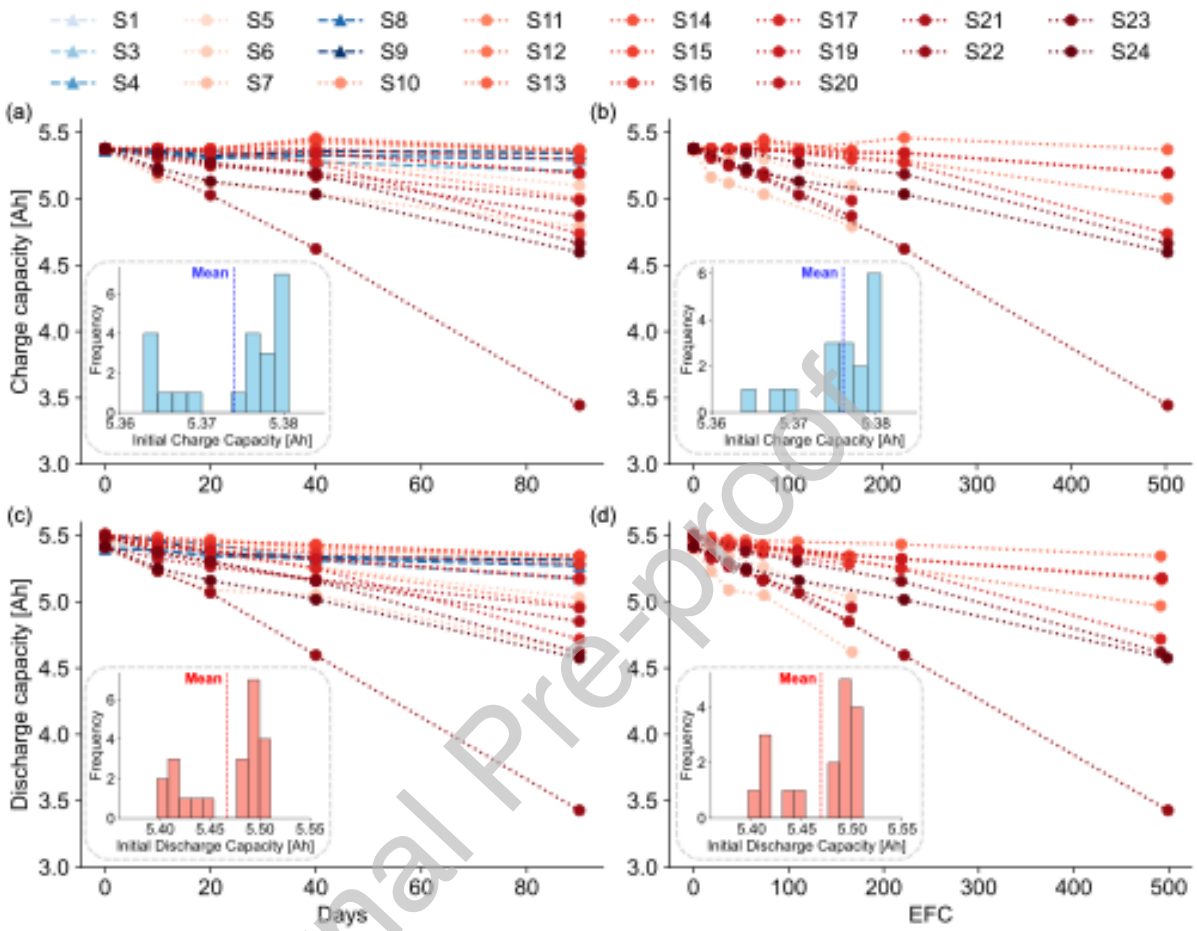

Figure 3: Capacity degradation curves in charge and discharge as functions of days and EFC. a) Capacity degradation curves in charge for all the cells show a similar starting capacity; however, as the cells degraded, the capacities showed a large spread. The histogram of initial charge capacity shows a bimodal distribution with more cells present above the mean. b) Capacity degradation curves for charge shows some cells undergoing more effective cycles, but the degradation is more dependent on the operating conditions used for aging. The distribution of initial charge capacity is a left-skewed distribution. c) Discharge capacity degradation curves show similar behaviour to (a). The initial discharge capacity distribution has a bimodal shape with more cells above the mean. d) Discharge capacity degradation curves with EFC shows similar trends to (b). The initial discharge capacity distribution remains bimodal despite removing calendar-aged cells.

During RPTs, EIS was performed to characterize the degradation of the cells. Fig. 4 shows the EIS curves for two cells: one calendar-aged and one cycle-aged. Fig. 4a shows the EIS for calendar-aged cell S8 at five different SOC points. The impedance was the largest at 0% SOC, but the variation in the EIS curves as the battery ages was small. For EIS curves at SOC at or above 25%, the overall impedance curves are smaller in magnitude, but the variation with aging was more pronounced. In general, the curves did not change significantly but rather moved towards the right as resistance increased with aging. Similarly, Fig. 4b shows the EIS curves for cycle-aged cell S22. The imaginary impedance at 0% SOC was substantially larger than at other SOC values. Furthermore, with aging, the difference in the EIS curves was apparent at all SOC values. In terms of the shape of the EIS curves, the curves at 0% SOC for both cells did not

Data in Brief
Open access
Article template

exhibit a clear semicircle, but a clear semicircle is present at all other SOC values for both cells. For Cell S22, the size of the semicircle also increased with aging, indicating an increase in charge transfer resistance. Based on the relative change in the EIS curves between S8 and S22, it is observed that the impact of cycle-aging is more prominent, leading to an increase in both charge transfer and diffusion resistance. This is apparent from the increase in the size of the semicircle and diagonal line for S22 with aging.

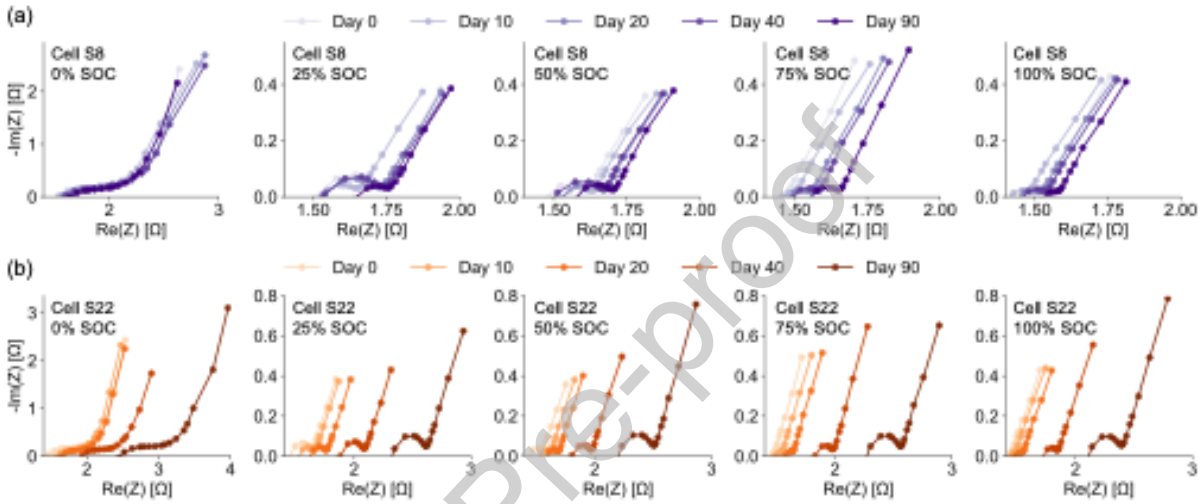

Figure 4: EIS curves for a) one calendar-aged cell S8 and b) one cycle-aged cell S22, both at five different SOC values. EIS curves for cell S8 in (a) show variation with calendar aging, with a general trend of shifting towards the right. The impedance at 0% SOC is significantly larger than the impedance at other SOC values. Similarly, EIS curves for cell S22 in (b) show a more apparent shift towards the right and an increase in the size of the semicircle with aging. For both cells, EIS at 0% SOC does not show a clear semicircle.

The high-frequency resistance R_0 is defined as the intersection point of the EIS curve with the real impedance axis and represents the electrolyte resistance present in the cell. Fig. 5a shows the variation of R_0 with aging. The boxplots move upwards with aging days indicating an increase in overall R_0. Furthermore, the spread of R_0 is also increasing with more outliers present at day 40 and day 90. This shows the impact of different operating conditions on the cell degradation, resulting in an increasing heterogeneity between the cells. On the other hand, Fig. 5b illustrates R_0 as a function of SOC, showing a decrease as SOC increases. The variation with SOC remained consistent, and outliers were present at all SOC values.

Fig. 5c shows the distribution of R_0 for fresh and day-90 cycle-aged cells. The fresh cells form a tight distribution between 1.4 and 1.5 mΩ, but at the end of the aging campaign, a large spread is observed, with the distribution skewing towards the right. The maximum R_0 appears close to 2.5 mΩ. Similarly, Fig. 5d shows the distribution of R_0 for calendar-aged cells. The fresh cell distribution is between 1.35 and 1.5 mΩ, but the distribution at day-90 shows a spread to approximately 1.75 mΩ. The day 90 distribution is symmetric and can be represented by a Gaussian distribution. Furthermore, the distribution at day 90 for calendar-aged cells does not have a spread as wide as the distribution for cycle-aged cells. This

Data in Brief
Open access
Article template

suggests that, despite variations in operating conditions for calendar aging, the impact on aging is not as severe as it is for cycle-aged cells, where a long tail appears in the R_0 distribution.

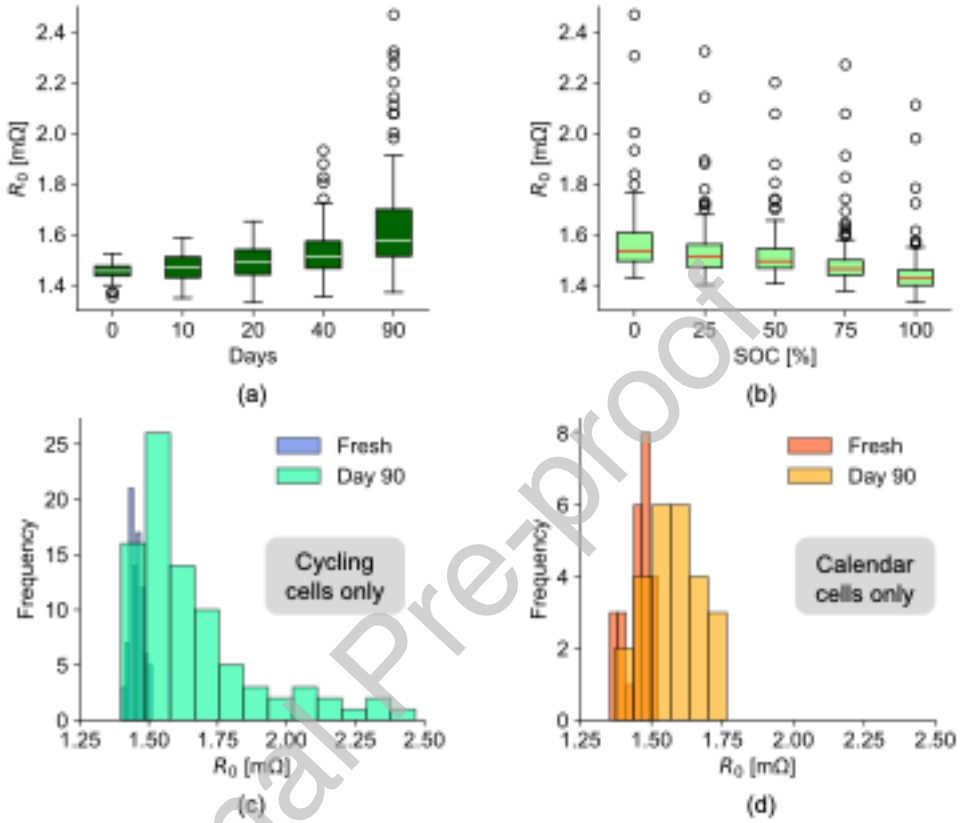

Figure 5: Variation of high-frequency resistance R_0. a) Boxplots of R_0 show an increase in R_0 with aging, along with an increase in the variation of R_0 values represented by the large box plot whiskers. b) Boxplots of R_0 with SOC show a slight decrease as SOC increases; however, the variation of R_0 values remains consistent with outliers present at all SOC values. c) Comparison of fresh and day-90 cycle-aged cells shows significant differences as the distribution limits change from 1.4-1.5 mΩ to 1.4-2.5 mΩ, indicating a large spread with aging. d) Similar comparison as (c) for calendar-aged cells showing a wider unimodal distribution on day 90 as compared to the fresh cell distribution. Between (c) and (d), the cycle-aged cells show a much larger change in the R_0 distribution at the end of the aging campaign.

1.1 Dataset structure

The dataset provided includes capacity and EIS data, as shown in Fig. 6.

The capacity_data folder contains Excel (*.xlsx*) spreadsheets of the capacity data for each cell from S1 through S24, with the exception of S2 and S18. Each *.xlsx* file is labeled CD_t25 _#d (with # = day 0, 10, 20, 40, or 90) or CDS_t25_#d (with # = day 70 or 90). This represents capacity data collected at 25 °C and at different RPT days. In addition, FCC.*xlsx* contains the full charge/discharge capacity and SOH data from each charge/discharge data file for each cell.

Data in Brief
Open access
Article template

Secondly, the EIS_data folder contains EIS data in two formats, *.csv* or *.xlsx*. Inside the *csv* folder, each folder is labelled S1 through S24, except S5, S6, and S7, for each cell. Each cell-specific folder contains EIS data from five SOCs and five RPTs. The *.csv* files are named ACR_t25_S$_#d_S1_convert.csv (where $ is the 0, 25, 50, 75, or 100 SOC and # is the day 0, 10, 20, 40, 70, or 90). S2 and S18 have limited data for only day 0, 10, and 20. Folders S5, S6, and S7 are structured differently. While they each contain a *t25* folder, which includes the same files as the folders for the other cells, they also include folders S0, S25, S50, S75, and S100, which contain EIS data from different SOCs, cell ages, and temperatures. These *csv* files are named ACRS_t&_s$_#d_S% (where & is the temperature, $ is the SOC, # is the day, and % is the cell).

The *xlsx* folder contains five subfolders named #d (where # is the day 0, 10, 20, 70, or 90). Each subfolder contains each EIS data file named ACR_t&_s$_#d or ACRS_t&_s$_#d (where & is the temperature, $ is the SOC, and # is the day).

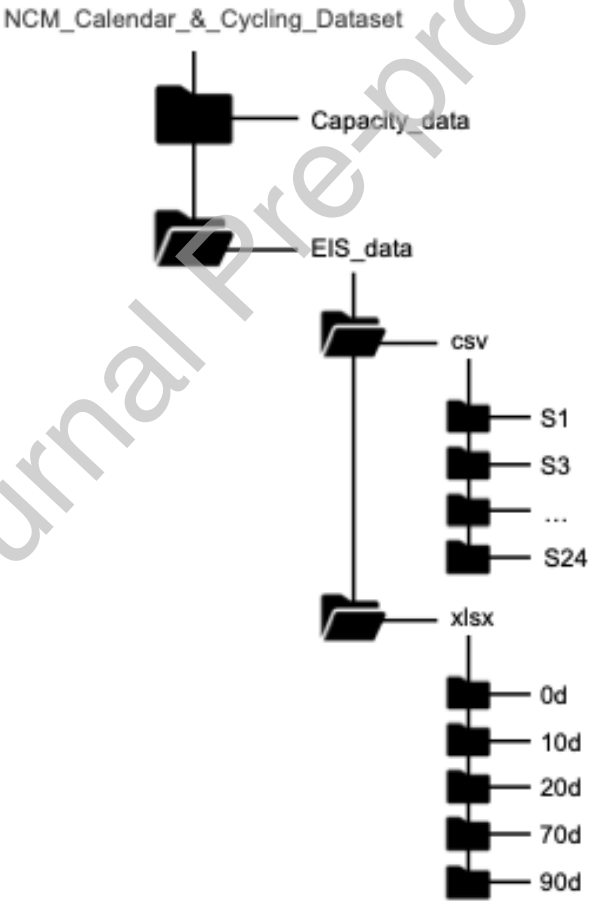

Figure 6: Dataset folder structure.

Data in Brief
Open access
Article template

EXPERIMENTAL DESIGN, MATERIALS AND METHODS

EIS data was obtained using a frequency response analyzer and potentiostat/galvanostat. The experimental setup included a host computer interfaced with the EIS instrument to facilitate data collection. For cycle aging and capacity tests, the battery cycler was used to supply current and measure cell voltage data. The tested NMC/graphite cells were placed inside a thermal chamber to ensure stable temperature conditions throughout testing.

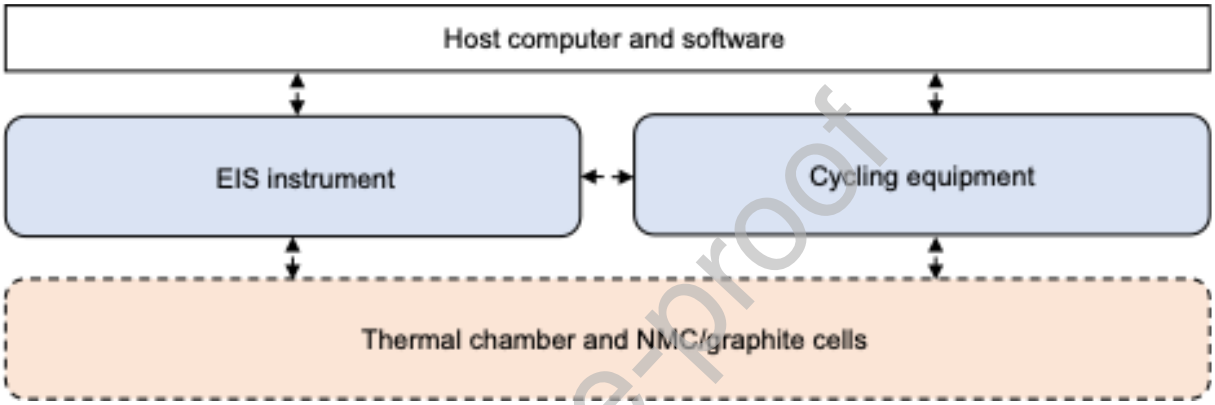

Figure 7: Representation of data collection equipment for the dataset in this work.

LIMITATIONS

This dataset offers a diverse set of aging conditions and multi-SOC EIS measurements; however, it has some limitations. The study spans 90 days, so long-term degradation mechanisms may not have been fully captured. Findings and models from this dataset of prismatic NMC/graphite cells may not be directly transferrable to other chemistries. Although aging was conducted at 0 °C, 25 °C, and 40 °C, all RPTs were performed at 25 °C. This may limit the observation of degradation effects that are only visible under low- or high-temperature testing. The exact location of the temperature sensors is unknown because the data collection was outsourced to KRI by our collaborators. Due to this, information about any possible thermal gradients is not available.

ETHICS STATEMENT

Hereby, we, Simona Onori, Muhammad Aadil Khan, and Colin Chu, assure that for the manuscript *Calendar and cycle aging dataset for lithium-ion batteries with multi-SOC electrochemical impedance spectroscopy measurements* the following is fulfilled:

- This material is the authors' own original work, which has not been previously published elsewhere.

- The paper is not currently being considered for publication elsewhere.
- The paper reflects the authors' own research and analysis in a truthful and complete manner.
- The results are appropriately placed in the context of prior and existing research.
- All sources used are properly disclosed. Literal copying of text must be indicated as such by using quotation marks and giving proper reference.
- All authors have been personally and actively involved in substantial work leading to the paper and will take public responsibility for its content.

CREDIT AUTHOR STATEMENT

Muhammad Aadil Khan: Software, Formal analysis, Investigation, Data Curation, Writing – Original Draft, Visualization, Writing – Review & Editing. **Colin Chu:** Software, Data Curation, Writing – Original Draft, Visualization, Writing – Review & Editing. **Simona Onori:** Writing – Review & Editing, Supervision, Funding acquisition.

ACKNOWLEDGEMENTS

The research presented in this paper is part of Stanford SystemX Initiative, in collaboration with Nuvoton Technology Corporation Japan (NTCJ). The authors would like to thank NTCJ for collecting this dataset. Additionally, the authors are thankful to Sai Thatipamula for his assistance in processing the dataset.

DECLARATION OF COMPETING INTERESTS

The authors declare that they have no known competing financial interests or personal relationships that could have appeared to influence the work reported in this paper.

REFERENCES

1. Khan, M. A., Thatipamula, S., & Onori, S. (2024). Onboard Health Estimation using Distribution of Relaxation Times for Lithium-ion Batteries. *IFAC-PapersOnLine*, *58*(28), 917-922.
2. Guo, J., Li, Y., Pedersen, K., & Stroe, D. I. (2021). Lithium-ion battery operation, degradation, and aging mechanism in electric vehicles: An overview. *Energies*, *14*(17), 5220.
3. Chu, C., Thatipamula, S., & Onori, S. (2025). Frequency-Based Parameterization of Semi-Empirical Models for State-of-Health Estimation in Lithium-Ion Batteries. *Journal of The Electrochemical* Society, Accepted.
4. B. Saha and K. Goebel (2007). NASA Prognostics Data Repository. https://www.nasa.gov/intelligent-systems-division/discovery-and-systems-health/pcoe/pcoe-data-set-repository/

5. Kollmeyer, P., Hackl, A., & Emadi, A. (2017, June). Li-ion battery model performance for automotive drive cycles with current pulse and EIS parameterization. In *2017 IEEE transportation electrification conference and expo (ITEC)* (pp. 486-492). IEEE.
6. Bessman, A., Soares, R., Wallmark, O., Svens, P., & Lindbergh, G. (2019). Aging effects of AC harmonics on lithium-ion cells. *Journal of Energy Storage*, *21*, 741-749.
7. Raj, T., Wang, A. A., Monroe, C. W., & Howey, D. A. (2020). Investigation of path-dependent degradation in lithium-ion batteries. *Batteries & Supercaps*, *3*(12), 1377-1385.
8. Gasper, P., Schiek, A., Smith, K., Shimonishi, Y., & Yoshida, S. (2022). Predicting battery capacity from impedance at varying temperature and state of charge using machine learning. *Cell Reports Physical Science*, *3*(12).
9. Goldammer, E., Gentejohann, M., Schlüter, M., Weber, D., Wondrak, W., Dieckerhoff, S., ... & Kowal, J. (2022). The impact of an overlaid ripple current on battery aging: The development of the sicwell dataset. *Batteries*, *8*(2), 11.
10. Mohtat, P., Lee, S., Siegel, J. B., & Stefanopoulou, A. G. (2021). Reversible and irreversible expansion of lithium-ion batteries under a wide range of stress factors. *Journal of The Electrochemical Society*, *168*(10), 100520.
11. Pozzato, G., Allam, A., & Onori, S. (2022). Lithium-ion battery aging dataset based on electric vehicle real-driving profiles. *Data in brief*, *41*, 107995.
12. Rashid, M., Faraji-Niri, M., Sansom, J., Sheikh, M., Widanage, D., & Marco, J. (2023). Dataset for rapid state of health estimation of lithium batteries using EIS and machine learning: Training and validation. *Data in Brief*, *48*, 109157.